Pergamon

Pattern Recognition, Vol. 31, No. 5, pp. 551–560, 1998

0031–3203/98 $19.00 + .00

PII: S0031-3203(97)00068-X

A MOMENT-PRESERVING APPROACH FOR DEPTH FROM DEFOCUS

DU-MING TSAI* and CHIN-TUN LIN

Department of Industrial Engineering, Yuan-Ze Institute of Technology, 135 Yuan-Tung Road, Nei-Li, Tao-Yuan, Taiwan, R.O.C.

(*Received* 10 *September* 1996; *accepted* 18 *June* 1997)

Abstract—For range sensing using depth-from-defocus methods, the distance D of a point object from the lens can be evaluated by the concise depth formula $D = P/(Q - d_b)$, where P and Q are constants for a given camera setting and d_b is the diameter of the blur circle for the point object on the image detector plane. The amount of defocus d_b is traditionally estimated from the spatial parameter of a Gaussian point spread function using a complex iterative solution. In this paper, we use a straightforward and computationally fast method to estimate the amount of defocus from a single camera. The observed gray-level image is initially converted into a gradient image using the Sobel edge operator. For the edge point of interest, the proportion of the blurred edge region p_e in a small neighborhood window is then calculated using the moment-preserving technique. The value of p_e increases as the amount of defocus increases and, therefore, is used as the description of degradation of the point-spread function. In addition to the use of the geometric depth formula for depth estimation, artificial neural networks are also proposed in this study to compensate for the estimation errors from the depth formula. Experiments have shown promising results that the RMS depth errors are within 5% for the depth formula, and within 2% for the neural networks.

Depth from defocus Range sensing Moment-preserving Neural networks

1. INTRODUCTION

Depth measurement is one of the most important tasks in computer vision for the applications of 3-D object recognition, scene interpretation and robotics. Various methods for depth measurement have been proposed.[1] Stereo vision[2, 3] is perhaps the most popular technique to obtain the depth image of a 3-D object. It generally uses two cameras to estimate stereo disparity and then recovers the 3-D structure of an object. The camera model of a stereo system involves a matching process between two images. This requires reliable extraction of features from the separate 2-D images and the matching of these features between images. Both of these tasks are non-trivial and can be computationally expensive.

In contrast to stereo vision, Pentland[4, 5] has proposed a depth-from-defocus (DFD) method to measure the depth information using a single camera so that the image-to-image correspondence process is not required. DFD methods are based on the fact that in the image formed by an optical system, objects at particular distance from the lens will be focused, whereas objects at other distances will be blurred by varying degrees depending on their distances. As the distance between the imaged point and the surface of exact focus increases, the imaged object becomes progressively more defocused. By measuring the amount of defocus (blur) of a point object in the observed image, the depth of the point object with respect to the lens can be recovered from the geometric optics.

The blur estimation algorithms generally determine the blur estimate from either the image's power spectrum in the frequency domain, or from the image's point-spread function in the spatial domain.[6] Pentland[7] has proposed two methods to measure the amount of defocus. The first method requires only one image and is based on measuring the blur of edges which are step discontinuity in the focused image. The blurred edge is modeled as the result of convolving a focused image with a point-spread function that is assumed to be a Gaussian distribution with spatial parameter σ. The parameter σ is used as the measure of defocus, and has a one-to-one correspondence to the depth. The second method requires two images and is based on comparing the two images formed with different aperture diameter settings. A ratio of the Fourier powers between the two images is shown to be related to the amount of defocus.

Following Pentland's second method, many blur estimation algorithms have been developed.[6, 8–11] These algorithms generally require two or more images obtained by changing one of the three intrinsic camera parameters: (1) distance between the lens and

* Author to whom correspondence should be addressed.

the image detector plane, (2) focal length of the lens, and (3) diameter of the lens aperture (*f*-number). These involve relatively low mechanical movement of the camera and need specialized camera system whose parameter setting can be controlled precisely.

Lai *et al.*[12] have proposed a generalized algorithm that follows Pentland's first method for estimating the spatial parameter σ of a Gaussian point-spread function. The spatial parameter σ is decomposed into the horizontal and vertical components σ_x and σ_y so that the estimation of the edge orientation is not required. The horizontal and vertical intensities of an observed edge is assumed to be the convolution of the focused image and the Gaussians with spatial parameters σ_x and σ_y, respectively. The blur estimation problem is then formulated as a nonlinear equation. The parameters σ_x and σ_y are evaluated using an iterative solution based upon Newton's method in the vicinity of piecewise linear edges. Since no closed-form solution exists for their model, the nonlinear search procedure can be very time-consuming and the solution may get stuck in some local minimum.

In this paper, we use the moment-preserving principle, which gives closed-form solution and is computationally fast, to estimate the amount of defocus from a single image. The basic framework of our approach is as follows. The observed gray-level image is initially converted into a gradient image using the Sobel edge operator. For every edge point of interest in the gradient image, the proportion of the edge region p_e in a small neighborhood window centered at the edge point is then computed using the moment-preserving method. A focused edge will result in small value of p_e, while a defocused edge will yield large value of p_e. The proportion of blurred edge p_e is, therefore, used as the description of degradation of the point-spread function for estimating the depth. In addition to the use of the depth formula derived from geometric optics for depth estimation, artificial neural networks (ANNs) are also proposed in this study to compensate for the estimation error from the depth formula.

This paper is organized as follows: Section 2 overviews the geometry of the depth formula. Section 3 describes the moment-preserving procedure for estimating the proportion of blurred edge region p_e in the neighborhood window. The ANNs used for compensating for the estimation error are discussed in Section 4. Section 5 presents the experimental results including the effect of varying sizes of the neighborhood window on estimation errors, and the depth accuracy of the geometric depth formula and the ANNs. The paper is concluded in Section 6.

2. THE DEPTH FORMULA

For a convex-lens camera with a lens of focal length F, the relation between the position of a point in the scene and the position of its focused image is given by the well-known lens law

$$\frac{1}{v} + \frac{1}{D} = \frac{1}{F}, \tag{1}$$

where D is the distance of the point object from the lens and v is the distance of the focused image from the lens.

Let o be a point object on a visible surface in the scene, and o' and o'' be its corresponding points in the focused image and the image-detector plane, respectively. If o is not in focus then it gives rise to a circular image called the blur circle on the image-detector plane (see Fig. 1). Let the diameter of the blur circle be denoted by d_b. Pentland[7] has shown that the relationship between the depth D of a point object and the diameter d_b of the blur circle is given by

$$D = \frac{Fv_0}{v_0 - F - d_b f} \quad \text{for } v_0 > v, \tag{2a}$$

$$D = \frac{Fv_0}{v_0 - F + d_b f} \quad \text{for } v_0 < v, \tag{2b}$$

where v_0 is the distance between the lens and the image-detector plane, and f is the f-number (aperture) of the lens system. As the sensor displacement increases (i.e., $v_0 - v$), the defocusing diameter d_b increases. Note that defocusing is observed for both positive and negative sensor displacement. If the image detector is behind the focused image (i.e. $v_0 > v$), the depth D is evaluated by equation (2a). If the image detector is in front of the focused image (i.e. $v_0 < v$), the depth D is then evaluated by equation (2b). For a given lens system, the parameters F, v_0 and f can be considered as constants. Therefore, equation (2) shows that the defocus d_b is an unique indicator of depth D. The depth formula of equation (2) can be rewritten in a condensed form[12] as follows:

$$D = \frac{P}{Q \pm d_b}, \tag{3}$$

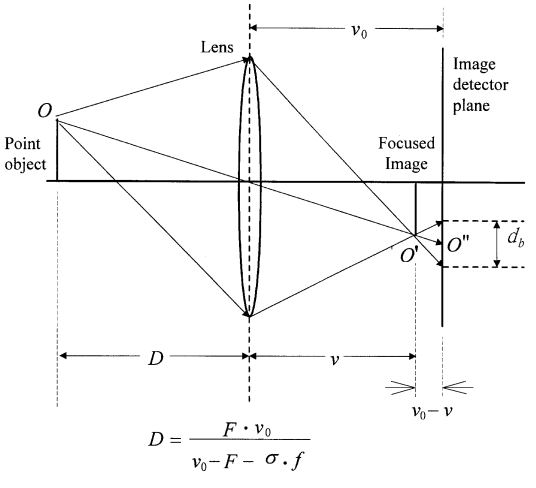

Fig. 1. Image formation and defocus in a convex lens.

where $P = Fv_0/f$, $Q = (v_0 - F)/f$, and P and Q are constants with respect to a given camera setting. The depth formulation of equation (3) can be used to simplify the calibration procedure.

3. MEASURE OF DEFOCUS

The depth formula of equation (3) shows that there is a one-to-one correspondence between the diameter of blur circle d_b and the object depth D. The blur size d_b is generally assumed to be proportional to the spatial parameter σ of the point-spread function, i.e. $d_b = k\sigma$ where k is assumed to be a constant for a given lens system.[7, 11–13] Quantitative measurement of defocus is difficult and requires accurate modeling of the point-spread function. Unlike the conventional blur estimation algorithms that assume the point-spread function is a Gaussian distribution with spatial parameter σ and solve for the value of σ in a complex way, we use a more straightforward approach to find the amount of defocus by the moment-preserving technique. The observed image is initially converted into a gradient image using the Sobel edge operator so that edge pixels have large gradient magnitude, and non-edge pixels have approximately zero gradient magnitude. For each edge point of interest, the proportion of the edge region p_e (i.e. the region with high gradient magnitude) with respect to the neighborhood window in the gradient image is computed using the moment-preserving principle. A focused edge will result in small p_e, whereas a defocused edge will yield large p_e. p_e increases as the distance between the imaged point and the surface of exact focus increases. Therefore, p_e is a measure for the amount of defocus. The estimation procedure for the proportion of edge region p_e in a small window is described in detail as follows.

Let $f(x, y)$ be the gray level of a pixel at (x, y) in the observed image. The gradient of $f(x, y)$ is given by

$$\nabla f(x, y) = \begin{bmatrix} g_x \\ g_y \end{bmatrix},$$

where

$$g_x = \sum_j \sum_i f(x + i, y + j) \cdot w_x(i, j),$$

$$g_y = \sum_j \sum_i f(x + i, y + j) \cdot w_y(i, j).$$

The horizontal and vertical Sobel edge operators $W_x(i, j)$ and $W_y(i, j)$, $-1 \le i, j \le 1$, are given in Fig. 2. The magnitude of the gradient is defined by

$$g(x, y) = |\nabla f(x, y)| = [g_x^2 + g_y^2]^{1/2}.$$

$g(x, y)$ forms the gradient image of the observed image $f(x, y)$. Figure 3(a) demonstrates the observed gray-level image of a multi-step block. The camera is focused on the lower steps of the block (lower-right in the image), and the upper steps are close to the lens and result in defocused image (upper-left in the image). Figure 3(b) presents the resulting gradient image of the observed image. It shows that the focused steps result in thin and sharp edges, and the defocused steps yield thick and scattering edges. The width of edges increases from lower-right to upper-left in the gradient image as the multi-step block is defocused progressively from lower steps to upper steps. The width of edges in the gradient image can be a description for the diameter of blur circle d_b.

-1	-2	-1
0	0	0
1	2	1

(a) $W_x(i, j)$

-1	0	1
-2	0	2
-1	0	1

(b) $W_y(i, j)$

Fig. 2. The horizontal and vertical Sobel edge operators.

As observed in Fig. 3(b), the gradient image can be divided into two regions, the bright region that represents the edges with high gradient magnitudes, and the dark region that represents the interior portions of objects or the background with low gradient magnitudes. Given a local neighborhood window centered at the edge point of interest, the gradient image defined in the window can be converted into a binary image that contains only white region (i.e. high gradient magnitude for edges) and black region (i.e. low gradient magnitude for backgrounds) using the moment preserving method. The proportion of the white region with respect to the entire window region represents the width of the imaged edge in the gradient image and, therefore, indicates the diameter of blur circle d_b.

Let the gradient image $g(x, y)$ defined in a local neighborhood window be the real-world version of an ideal gradient image that consists of only two homogeneous regions, the bright region with a uniform gradient magnitude h_e, and the dark region with a uniform gradient magnitude h_b. Denote p_e and p_b by the proportions of the bright region and the dark region, respectively, in the ideal gradient image. Note that $h_e > h_b$, $0 \le p_e$, $p_b \le 1$ and $p_e + p_b = 1$. For a given edge point at (x, y), the first three moments of $g(x, y)$ are given by

$$m_j = \frac{1}{n} \sum_{(s, t) \in N(x, y)} [g(s, t)]^j, \quad j = 1, 2, 3,$$

where $N(x, y)$ is the neighborhood window that consists of neighboring points around (x, y), and n is the total number of pixels in the window.

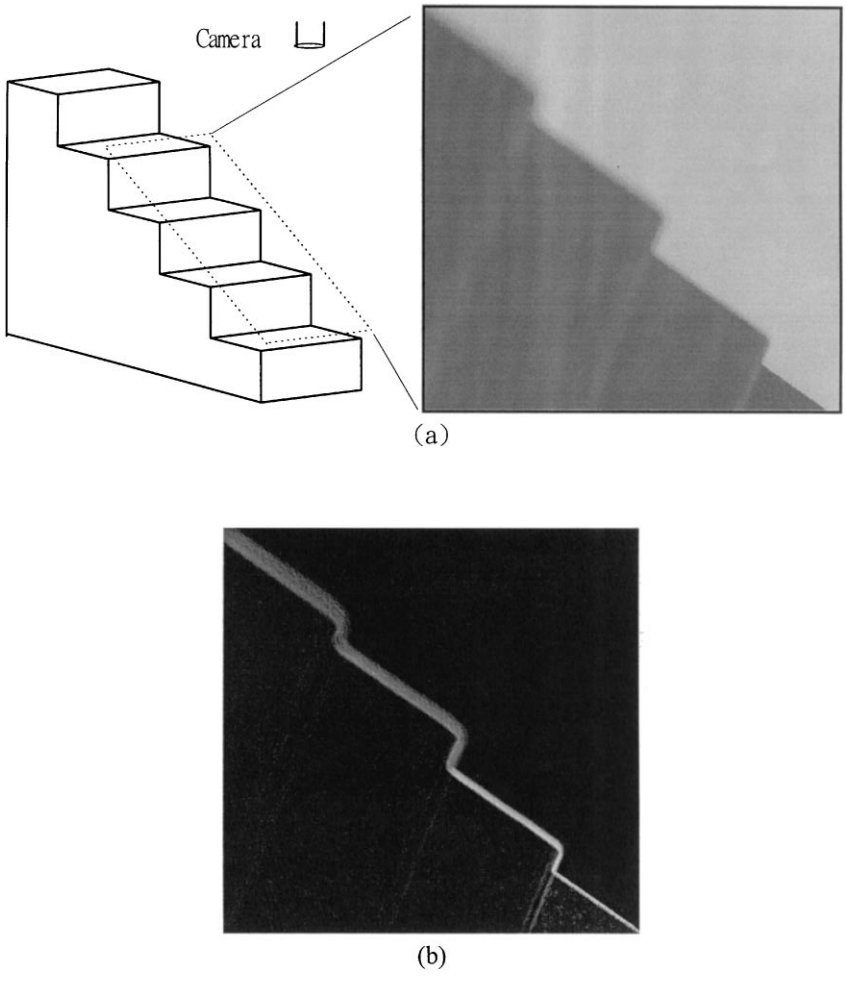

Fig. 3. Images of a multi-step block. (a) The original gray-level image. (b) The corresponding gradient image. The camera is focused on the top of the table where the block is located.

By preserving the first three moments in both real-world gradient image $g(x, y)$ and the ideal gradient image, we can obtain four equations as follows:

$$p_e h_e^1 + p_b h_b^1 = m_1,$$
$$p_e h_e^2 + p_b h_b^2 = m_2,$$
$$p_e h_e^3 + p_b h_b^3 = m_3$$

and

$$p_e + p_b = 1.$$

There exists a closed-form solution for the four unknown variables p_e, p_b, h_e and h_b, which are given by[14]

$$h_b = \tfrac{1}{2}[-c_1 - (c_1^2 - 4c_0)^{1/2}],$$
$$h_e = \tfrac{1}{2}[-c_1 + (c_1^2 - 4c_0)^{1/2}],$$
$$p_b = \begin{vmatrix} 1 & 1 \\ m_1 & h_e \end{vmatrix} \Big/ \begin{vmatrix} 1 & 1 \\ h_b & h_e \end{vmatrix},$$
$$p_e = 1 - p_b,$$

where

$$c_0 = \begin{vmatrix} -m_2 & m_1 \\ -m_3 & m_2 \end{vmatrix} \Big/ (m_2 - m_1^2),$$

$$c_1 = \begin{vmatrix} 1 & -m_2 \\ m_1 & -m_3 \end{vmatrix} \Big/ (m_2 - m_1^2).$$

The value of p_e, $0 \le p_e \le 1$, gives the proportion of edge region in the neighborhood window. The larger the value of p_e, the larger the amount of defocus. In this study, p_e is assumed to be proportional to the diameter of blur circle d_b, i.e. $d_b = kp_e$, where k is a constant. Therefore, the depth formula derived in equation (3) can be rewritten as

$$D = \frac{P'}{Q' \pm p_e}, \tag{4}$$

where $P' = kFv_0/f$, $Q' = k(v_0 - F)/f$, and P' and Q' are constants for a given camera setting.

The constants P' and Q' in equation (4) can be determined initially once and for all by a suitable camera calibration. We may manually collect n data points of the measured depths D_i, $i = 1, 2, \ldots, n$, at different distances from the camera, and use the moment-preserving method to calculate their corresponding proportions of edge region p_{e_i} in the local window. Let $\underline{D} = (D_1, D_2, \ldots, D_n)^{\mathrm{T}}$ and $\underline{p_e} = (p_{e_1}, p_{e_2}, \ldots, p_{e_n})^{\mathrm{T}}$. $(\underline{D}, \underline{p_e})$ gives a set of n known data pairs. Then, the best estimates of P' and Q', in the least-squares sense, are given by

$$\begin{bmatrix} Q' \\ P' \end{bmatrix} = [\underline{D} \ -1]^{\mathrm{T}}([\underline{D} \ -1] \cdot [\underline{D} \ -1]^{\mathrm{T}})^{-1} \cdot \underline{C},$$

where $\underline{C} = (D_1 \cdot p_{e_1}, D_2 \cdot p_{e_2}, \ldots D_n \cdot p_{e_n})$. Once P' and Q' are fixed for a given camera setting, the numerical relationship between the depth D and p_e is uniquely determined by equation (4).

4. ANN APPROACH FOR ERROR COMPENSATION

Since the depth formula of equation (3) arises from the geometric optics of lens imaging, the diameter of blur cycle d_b only represents the geometric blur. However, the actual blur is not due to geometric defocus alone.[15] The geometric depth formula may yield nonlinear errors in calculating the depth D owing to optical aberrations, vignetting, etc. To overcome this problem, we use artificial neural networks (ANNs) to compensate for the errors resulted from the depth formula. The advantages of an ANN in estimation applications are that it provides a model-free approach to reducing the estimation error, and it generates nonlinear interpolation for input data which are previously unseen in training.

An ANN is specified by the topology of the network, the characteristics of the nodes and the processing algorithm. The neural networks used in this work are multilayer feedforward neural networks composed of an input layer, a single hidden layer, and an output layer. Each layer is fully connected to the succeeding layer. The outputs of nodes in one layer are transmitted to nodes in another layer through links. The link between nodes indicates flow of information during recall. During learning, information is also propagated back through the network and used to update connection weights between nodes.

Let o_j be the output of the previous layer and w_{ij} the connection weight between the ith node in one layer and jth node in the previous layer. The total input to the ith node of a layer is

$$\mathrm{net}_i = \sum_j w_{ij} o_j.$$

A hyperbolic tangent activation function is used here to determine the output of the node i, which is given by

$$o_i = f(\mathrm{net}_i) = \frac{e^{\mathrm{net}_i} - e^{-\mathrm{net}_i}}{e^{\mathrm{net}_i} + e^{-\mathrm{net}_i}}.$$

In the learning phase for such a network, we present the training pattern $T = \{I_p\}$, where I_p is the pth node in the input layer, and ask the network to adjust the weights in all the connecting links such that the desired outputs $\{D_k\}$ are obtained at the output nodes. Let $\{O_k\}$ be the evaluated outputs of the network in its current state. For a training pattern the squared error of the system can be written as

$$E = \frac{1}{2}\sum_k (D_k - O_k)^2.$$

The generalized delta-rule learning algorithm[16] is applied to adjust the weights such that the error E is a minimum. A detailed derivation of the learning procedure can be found in reference (17).

Two neural networks are developed in this study. The first neural network, denoted by ANN_1, is a three-layer back-propagation network with two nodes in the input layer, seven nodes in the hidden layer, and one single node in the output layer. The topology of the network ANN_1 is illustrated in Fig. 4. The input vector $T_1 = (p_e, D)$ of the network ANN_1 includes two components, which are

p_e = the proportion of edge region in the neighborhood window obtained from the moment-preserving method.
D = the depth of an edge point derived from the depth formula of equation (4).

(p_e, D) correspond to the two nodes in the input layer in sequence. In the learning phase of the network, the desired value of the node in the output layer is the actual depth D^* known *a priori*. A pair of (Input, Output) = (T_1, D^*) forms the training sample for the network. In the recall phase of the network, the measured depth is simply given by the value of the node in the output layer.

It has been found[13] that the edge orientation is crucial to the estimation of the amount of defocus. A good strategy for improving the estimation accuracy of depth is to calibrate the constants P' and Q' in equation (4) using known data points in separate

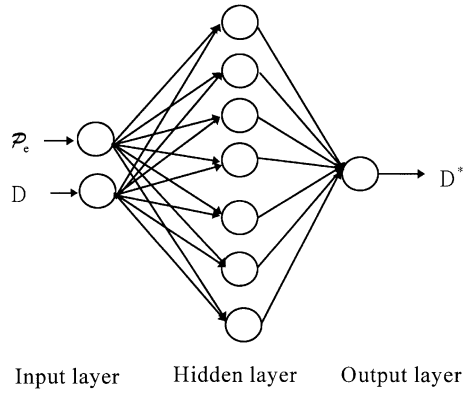

Fig. 4. The system architecture of the network ANN_1.

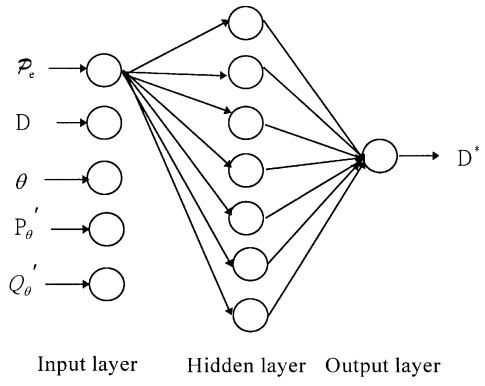

Fig. 5. The system architecture of the network ANN_2. (Only partial connections are presented.)

orientations, and then present the information of edge orientations to the network. The gradient $\nabla f(x, y) = (g_x, g_y)$ used for computing the gradient magnitude as described in Section 3 provides the additional information of edge orientation. The orientation of an edge point with gradient (g_x, g_y) is given by

$$\theta = \tan^{-1}\left(\frac{g_y}{g_x}\right). \tag{5}$$

The value of θ along with the signs of g_x and g_y can uniquely define the edge orientation between 0 and 360°.

The proposed second neural network, denoted by ANN_2, therefore takes the edge orientation, and constants P' and Q' calibrated in individual orientations as the additional input. The topology of the network ANN_2 is the same as that of the ANN_1, except that ANN_2 has five nodes in the input layer. The topology of the network ANN_2 is shown in Fig. 5. The input vector $T_2 = (p_e, D, \theta, P'_\theta, Q'_\theta)$ of the network ANN_2 consists of five components, which are

p_e, D = the same as those defined previously for the network ANN_1
θ = the edge orientation given by equation (5)
P'_θ, Q'_θ = the constants in equation (4) calibrated in the orientation of θ.

In the training phase of the network ANN_2, pairs of (T_2, D^*) form the training samples with finite number of edge orientations. In the recall phase of the network, the edge orientation evaluated by equation (5) is converted to the nearest orientation θ used in training, and the corresponding P'_θ and Q'_θ are selected from a look-up table. The value of the node in the output layer of the network gives the depth of the edge point.

5. EXPERIMENTAL RESULTS

In this section we present experimental results for evaluating the performance of the proposed depth estimators. In our implementations, all algorithms are programmed in the C language and executed on a personal computer with a Pentium 66 MHz processor. The image size is 512×480 pixels with 256 gray levels. The camera is set up so that the camera is 415 mm from the tabletop, and the optical axis of the camera is perpendicular to the table surface. All experiments are performed with the point of sharpest focus approximately set at the top of the table. A three-step block as shown in Fig. 6 is used as the benchmark in the experiments to evaluate the performance of the proposed depth estimators. The first step (the one closest to the table), the second step and the third step (the one closest to the camera) are 21, 40 and 40 mm in deep, respectively.

The first series of experiments use the three-step block to evaluate the effect of varying sizes of the neighborhood window on estimation errors of depth. The neighborhood window selected in this work is of circular shape. Figure 7(a) depicts the p_e value versus the depth of each step of the block for the neighborhood windows of radii 45, 35, 25 and 19 pixels. It can be seen from the figure that the value of p_e increases as the depth decreases, i.e. the amount of defocus increases as the object gets closer to the camera. The root-mean-squares (RMS) depth errors obtained by the depth formula for individual radii of the neighborhood windows are presented in Fig. 7(b). It shows that too small the size of the window may not include sufficient data to estimate p_e reliably, whereas too large the size of the window may include superfluous data and increases the computational requirement. Based on the experimental results, the neighborhood window of radius 35 pixels is valid for accurate estimation of p_e, and is used in the subsequential experiments.

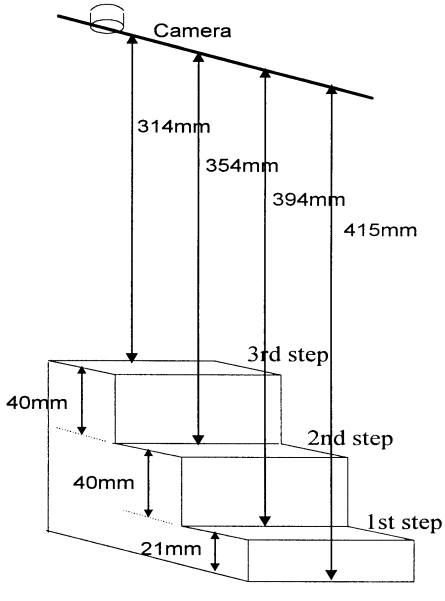

Fig. 6. A three-step block used for experiments.

(a)

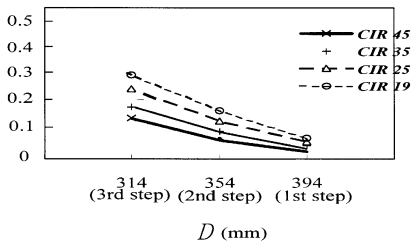

(b)

Radius of window (pixels)	45	35	25	19
RMS depth error (%)	2.55	2.41	4.02	5.45

Fig. 7. (a) The plots of the proportion of edge region p_e against the depth D for varying sizes of windows. (b) The measured errors of depth for varying sizes of windows.

The second series of experiments are to use the three-step block to evaluate the performances of the geometric depth formula and the neural networks ANN_1 and ANN_2. In order to analyze the effect of heights and orientations of objects with respect to a fixed camera, we have experimented the block placed at seven heights with respect to the tabletop varying from 0 to 60 mm in 10 mm increments. The block at each of the seven heights is rotated through eight orientations in approximately 45° increments. For each image of the block at a given height and orientation, we select two edge points from each step of the block as the test samples. Figure 8 shows the images of the three-step block at seven different heights. Of the seven heights, data sampled from the heights 0, 20 and 50 mm are used for both calibrating the constants P' and Q' in equation (4), and training the neural networks ANN_1 and ANN_2. Data sampled from the heights 10, 30, 40 and 60 mm are used for testing the estimation accuracy of the depth formula of equation (4) and the compensation capability of ANN_1 and ANN_2. Therefore, a total of 336 (3 steps × 2 edge points per step × 7 heights × 8 orientations) samples is generated. Of the 336 samples, 144 are used as the training patterns, and the remaining 192 untrained samples are used as the test set.

Furthermore, in order to evaluate the effect of gray-level contrasts on the estimation accuracy of depth, we have also experimented the placement of the three-step block on two backgrounds with distinct gray levels. The average gray level of the block in the image is 100, and the average gray-levels of the two backgrounds used in the experiments are 202 and 145. The block on the background with gray-level 202 is referred to as a high-contrast image, whereas the block on the background with gray-level 145 is referred to as a low-contrast image. Each contrast category contains 336 samples generated as described above. These two contrast categories generate following four combinations of experiments: (1) Both training samples and test samples are collected from high-contrast images, denoted by $E(H, H)$, (2) Training samples are generated from low-contrast images, but test samples are collected from high contrast images, denoted by $E(L, H)$, (3) Both training samples and test samples are generated from low-contrast images, denoted by $E(L, L)$, and (4) Training samples are generated from high-contrast images, but test samples are collected from low-contrast images, denoted by $E(H, L)$.

Now we evaluate the performance of the proposed depth estimators under two conditions: (1) calibrating and training the system without using the information of edge orientations, and (2) calibrating and training the system with the information of edge orientations.

Let the constants P' and Q' in equation (4) be calibrated, and the network ANN_1 be trained by the 144 known data samples without considering the information of edge orientations. Table 1 summarizes the experimental results of the root-mean-squares (RMS) depth errors in percentage for the geometric depth formula and the network ANN_1. It can be seen from Table 1 that the experiment of $E(H, H)$ gives the best performance with the RMS error of 1.77% from the depth formula. The proposed methods also work well when the training environment does not coincide with the testing environment. The experiment $E(L, H)$ compares favorably with the experiment $E(H, L)$, and even the experiment $E(L, L)$. The performance of the experiment $E(L, H)$ is as good as that of the experiment $E(H, H)$ if the network ANN_1 is applied. Therefore, in an application of the proposed methods for accurate depth estimation, high-contrast images with the same training environment and scene environment should be employed if the scene environment can be easily controlled. If the scene environment cannot be predicted beforehand, the use of relatively low-contrast images in training is a good strategy to generate good depth estimation.

The neural network approach with the network ANN_1 generally yields better depth estimation, especially for the experiments $E(H, L)$, $E(L, L)$ and $E(L, H)$, compared with the geometric depth formula. In general, the RMS error from the depth formula is within 5%, and the RMS error from the network ANN_1 is within 3% for the camera at 415 mm distance. These results compare competitively with the measured errors reported in references (10, 12, 18).

Now let the constants P' and Q' in equation (4) be separately calibrated using the known data samples in each edge orientation. Table 2 presents the experimental results of the RMS depth errors in percentage from the geometric depth formula and the network ANN_2 that uses the additional information of edge orientations as the input. The trend resulting from the experiments in Table 2 are consistent with that in Table 1. The experiment $E(H, H)$ yields the best performance with the RMS error of 0.64% from the network ANN_2. The experiment $E(L, H)$ yields twofold improvement over the experiment $E(H, L)$ when

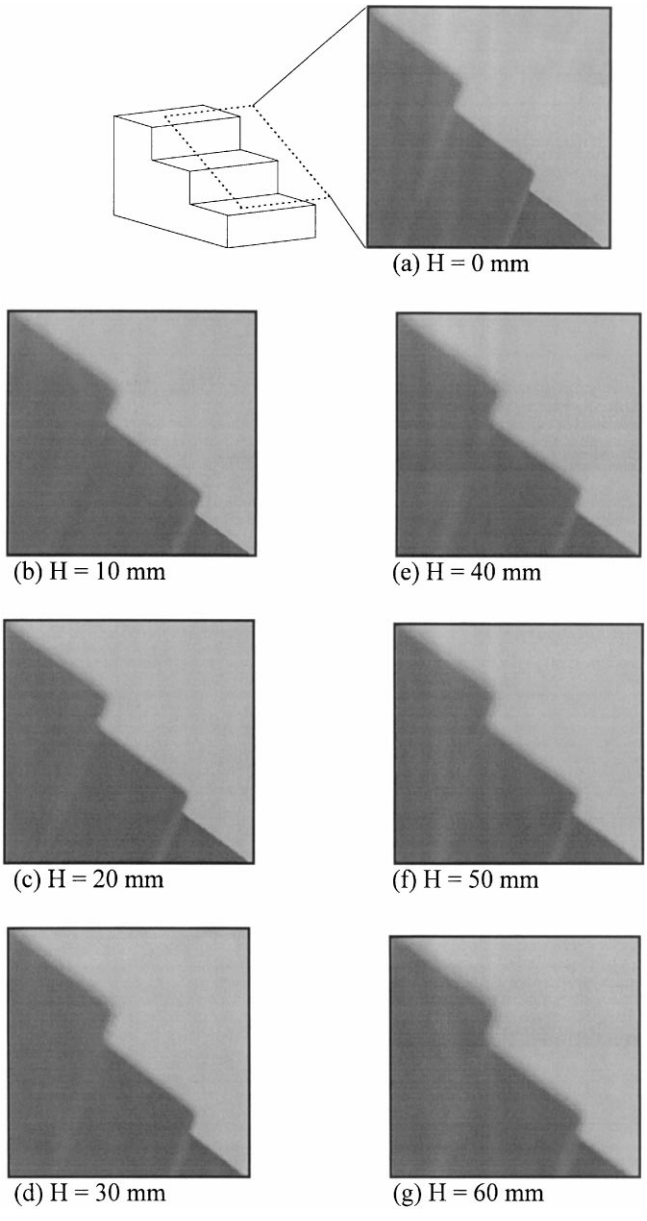

Fig. 8. The images of the three-step block at seven different heights. H represents the distance from the base of the block to the top of the table.

the training environment does not coincide with the scene environment.

The network ANN_2 works extremely well even for low-contrast images and non-coincident environments in training and testing. The improvement of the network ANN_2 versus the depth formula is about twofold. Given that the depth formula is used for estimating the depth in the experiments, the use of additional information of edge orientations for training individual P' and Q' does not generate significant improvement in the measured depth errors. However, if the neural network approach is used for measuring the depth in the experiments, the network ANN_2 that uses edge orientations to the input layer yields significant improvement in the measured errors, compared with the network ANN_1 that does not use the information of edge orientations as the input. In general, the RMS error from the geometric depth formula is still within 5% even with the information of edge orientations, and the RMS error from the network ANN_2 is within 2% as seen in Table 2. Based on the experimental results described above, the proposed moment-preserving method for estimating the proportion of edge region p_e and the proposed neural network approach have demonstrated their efficiency and effectiveness for edge-based depth estimation.

Table 1. Comparison of RMS depth errors from the depth formula and the network ANN_1 under different gray-level contrasts for training and testing. (The information of edge orientations is not applied.)

Experiment	RMS depth error (%)	
	Depth formula	Network ANN_1
$E(H, H)$	1.77	1.97
$E(L, H)$	3.25	1.97
$E(L, L)$	4.16	2.75
$E(H, L)$	4.27	2.75

Table 2. Comparision of RMS depth errors from the depth formula and the network ANN_2 under different gray-level contrasts for training and testing. (The information of edge orientations is utilized.)

Experiment	RMS depth error (%)	
	Depth formula	Network ANN_1
$E(H, H)$	1.22	0.64
$E(L, H)$	2.88	1.00
$E(L, L)$	4.06	1.52
$E(H, L)$	4.16	2.00

6. CONCLUSIONS

In this paper, the geometric depth formula is described by $D = P'/(Q' \pm p_e)$, where P' and Q' are constants for a given camera setting, and p_e is the proportion of edge region in a small neighborhood window. To compute the value of p_e, the original gray-level image is converted into a gradient image using the Sobel edge operator. For each edge point of interest in the gradient image, the proportion p_e is then evaluated using the moment-preserving principle. The moment-preserving method provides a closed-form solution to obtain the value of p_e, and is computationally fast. The resulting value of p_e is between 0 and 1, and increases as the amount of defocus increases. In addition to estimating the depth by using the geometric depth formula, two artificial neural networks ANN_1 and ANN_2 are also proposed in this study to compensate for the estimation error of the depth formula.

The best depth accuracy is obtained for objects in high-contrast images where the training environment coincides with the scene environment. The proposed methods also work well for objects that their training images and scene images have different gray-level contrasts. Experimental results have shown that the RMS error from the geometric depth formula is within 5%, and the RMS errors from the networks ANN_1 and ANN_2 are within 3 and 2%, respectively.

The interior edge that distinguishes between two homogeneous surfaces of an object generally has very low gradient magnitude in the gradient image. Since the proposed moment-preserving approach is based on the measurement of the proportion of edge region p_e in a local window in the gradient image, this restricts the proposed method in its current form to be only applicable to the edges between objects and the background.

REFERENCES

1. Y. Shirai, *Three-Dimensional Computer Vision*, Springer, Berlin (1987).
2. Y. C. Shah, R. Chapman and R. B. Mahani, A new technique to extract range information from stereo images, *IEEE Trans. Pattern Anal. Machine Intell.* **11,** 768–781 (1989).
3. N. Alvertos, D. Brzakovic and R. C. Gonzalez, Camera geometries for image matching in 3-D machine vision, *IEEE Trans. Pattern Anal. Machine Intell.* **11,** 897–915 (1989).
4. A. P. Pentland, Depth of scene from depth of field, *Proc. DARPA Image Understanding Workshop*. Palo Alto, CA (1982).
5. A. P. Pentland, A new sense for depth of field, *Proc. Int. Joint Conf. Artificial Intelligence*. Los Angels, CA (1985).
6. L. F. Hofeva, Range estimation from camera blur by regularized adaptive identification, *Int. J. Pattern Recog. Artificial Intell.* **8,** 1273–1300 (1994).
7. A. P. Pentland, A new sense for depth of field, *IEEE Trans. Pattern Anal Machine Intell.* **PAMI-9,** 523–531 (1987).
8. M. Subbarao, Direct recovery of depth map I: differenial methods, *Proc. IEEE Computer Soc. Workshop on Computer Vision.* Miami Beach (1987).
9. J. Ens and P. Lawrence, An investigation of methods for determining depth from focus, *IEEE Trans. Pattern Anal. Machine Intell.* **15,** 97–107 (1993).
10. M. Subbarao and G. Surya, Depth from defocus: a spatial domain approach, *Int. J. Comput. Vision* **13,** 271–294 (1994).
11. S. K. Nayar and Y. Nakagawa, Shape from focus, *IEEE Trans. Pattern Anal. Machine Intell.* **16,** 824–831 (1994).
12. S. -H. Lai, C. -W. Fu, A generalized depth estimation algorithm with a single image, *IEEE Trans. Pattern Anal. Machine Intell.* **14,** 405–411 (1992).
13. M. Subbarao and N. Gurumoorthy, Depth recovery from blurred edge, *IEEE Int. Conf. Computer Vision Pattern Recognition.* Ann Arbor, MI (1988).
14. W. -H. Tsai, Moment-preserving thresholding: a new approach, *Comput. Vision Graphics Image Process.* **29,** 377–393 (1985).
15. S. Xu, D. W. Capson and T. M. Caelli, Range measurement from defocus gradient, *Machine Vision Appl.* **8,** 179–186 (1995).
16. D. E. Rumelhart, G. E. Hinton and R. J. Williams, Learning internal representations by error propagation, *Parallel Distributed Processing: Explorations in the Microstructures of Cognition*, D. E. Rumelhart and J. L. McCelland (eds), Vol. 1, Foundations. MIT Press, Cambridge, MA (1986).
17. Y. -H. Pao, *Adaptive Pattern Recognition and Neural Networks*. Addison-Wesly, Reading, MA (1989).
18. A. Pentland, T. Darrell, M. Turk and W. Huang, A simple, real time range camera, *Proc. IEEE Comput. Soc. Conf. Computer Vision and Pattern Recognition.* San Diego, CA (1989).

About the Author—DU-MING TSAI received his B.S. degree in Industrial Engineering from the Tunghai University, Taiwan, R.O.C. in 1981, and the M.S. and Ph.D. degrees in industrial Engineering from Iowa State University, Ames, lowa in 1984 and 1987, respectively. From 1988 to 1990, he was a Principal Engineer of Digital Equipment Corporation, Taiwan branch, where his work focused on process and automation research and development. Currently he is a Professor of Industrial Engineering at the Yuan-Ze institute of Technology, Taiwan. His research interests include object representation, occluded object recognition, texture analysis and automated visual inspection.

About the Author—CHIN-TUN LIN received his B.S. degree in Applied Mathematics from the Chinese Culture University, Taiwan in 1990, and the M.S. degree in Industrial Engineering from the Yuan-Ze Institute of Technology, Taiwan in 1996. Currently, he is an automation engineer of Hon Hai Precision Industry Co., Ltd., Taiwan.